Jül-4368

Institut für Energie- und Klimaforschung
Plasmaphysik (IEK-4)

Stability of iterated plasma edge transport solvers

Heinke Frerichs

Member of the Helmholtz Association

JÜLICH
FORSCHUNGSZENTRUM

Stability of iterated plasma edge transport solvers

Heinke Frerichs

Berichte des Forschungszentrums Jülich; 4368
ISSN 0944-2952
Institut für Energie- und Klimaforschung
Plasmaphysik (IEK-4)
Jül-4368

Vollständig frei verfügbar im Internet auf dem Jülicher Open Access Server (JUWEL)
unter http://www.fz-juelich.de/zb/juwel

Zu beziehen durch: Forschungszentrum Jülich GmbH · Zentralbibliothek, Verlag
D-52425 Jülich · Bundesrepublik Deutschland
☎ 02461 61-5220 · Telefax: 02461 61-6103 · e-mail: zb-publikation@fz-juelich.de

Abstract

The application of numerical transport solvers for the plasma boundary of magnetic fusion devices is related to the iterative approximation of a fixed-point of a non-linear map. 2D (axisymmetric) or even 3D transport solvers are routinely applied for the quantification of steady state plasma flows. However, unstable behavior is found under certain conditions. A simple two-point model is applied to demonstrate that this kind of unstable behavior can occur when the fixed-point looses stability, resulting in a period doubling route to chaos. Furthermore, wavelike oscillations can occur at low temperatures. An adaptive relaxation scheme is presented which allows to suppress discrete and wavelike oscillations in order to stabilize the fixed-point iteration.

Die Anwendung von numerischen Transportlösern für die Plasmarandschicht in Fusionsanlagen mit magnetischem Einschluss ist verwandt mit der iterativen Approximation eines Fixpunktes einer nicht-linearen Abbildung. 2D (achsensymmetrisch) oder sogar 3D Transportlöser werden routinemäßig zur Quantifizierung von stationären Plasmaströmungen eingesetzt. Allerdings zeigt sich unter bestimmten Bedingungen instabiles Verhalten. Ein einfaches Zwei-Punkt Modell wird angewandt, um zu demonstrieren dass diese Art von instabilem Verhalten auftreten kann, wenn der Fixpunkt seine Stabilität verliert und sich auf einer Periodenverdopplungs-Route ins Chaos befindet. Zusätzlich können bei niedrigen Temperaturen wellenartige Oszillationen auftreten. Ein adaptives Relaxierungsverfahren wird vorgestellt welches diskrete und kontinuierliche Oszillationen unterdrücken kann um so die Fixpunkt-Iteration zu stabilisieren.

Contents

1. Introduction **7**

2. Two-point model analysis of iterated transport solvers **11**
2.1. Linearization 12
2.2. Convergence analysis 13
2.2.1. Example 1: The basic two-point model 13
2.2.2. Example 2: The extended two-point model 17
2.2.3. Implications for 2D/3D simulations 22

3. Convergence control by adaptive relaxation **25**
3.1. Control scheme for discrete oscillations 25
3.2. Control scheme for continuous oscillations 26
3.2.1. Last occurence of extremal values 27
3.2.2. Averaging of extremal values 27
3.3. Outlook to further advancements 33

4. Conclusions **37**

A. EMC3-EIRENE **39**

1. Introduction

The quantification of particle, momentum and energy fluxes in the domain near plasma exposed surfaces (in particular the divertor targets) is a key topic for the development of a magnetically confined fusion reactor. These fluxes can significantly affect the lifetime of plasma facing components, and hence, their control poses one of the major challenges for the successful operation of the next step fusion device ITER [1]. Of particular interest are so called *detached* plasma states which are characterized by a high density and low temperature in front of the divertor targets. Computer simulations of the plasma boundary both guide the interpretation of present fusion experiments and aid the design activities for future devices. Various computational edge transport models of diverse complexity have been developed in the past and are now routinely applied for the quantification of plasma flows. These have to deal with a large number of issues inherent to the physics of hot, ionized and magnetized plasmas: e.g. extreme anisotropy (transport time scales parallel and perpendicular to the magnetic field differ by several orders of magnitude) and strong non-linearity (i.e. the parallel heat conductivity κ scales as temperature $T^{5/2}$).

Toroidal symmetry is often assumed in computational models for tokamak configurations (the next step fusion device ITER is based on such a configuration), which allows to reduce the complexity of the numerical problem to two spatial dimensions. Furthermore, the plasma boundary is often assumed to be fairly collisional. This allows to derive and solve balance equations for particles, momentum and energy in ordinary space, instead of a more sophisticated kinetic treatment in phase space. Nevertheless, kinetic corrections by 'flux-limit factors' for lower collisionalities can be applied [2]. While the classical transport theory [3] provides an adequate approach for the transport along magnetic field lines, so-called anomalous transport across field lines is taken into account by a diffusion type ansatz. One such computational model is the B2-EIRENE code [4], also referred to as SOLPS. Its validation process includes benchmarks with other edge code [5] and it has meanwhile been established as a numerical tool for the performance analysis of the ITER divertor (see [6] and references therein).

However, despite the establishment of two dimensional models, three dimensional (3D) models have gained importance over the last years. This is because stellarator configurations (an alternative concept for the magnetic confinement) are intrinsically non-axisymmetric and have to be treated by 3D models, and furthermore because 3D effects can play a role in tokamak configurations as well. The tokamak operation with high confinement (H-mode [7]) is accompanied by edge localized instabilities (ELMs) which are considered a major threat for the plasma facing components in ITER [8]. Because

of the recent success in controlling ELMs by resonant magnetic perturbations (RMPs) from external coils [9, 10, 11, 12], ELM control coils are integrated in the latest ITER design as well [13]. The EMC3-EIRENE code [14, 15], which has originally been developed for stellarators and later adapted to poloidal divertor configurations [16], is a 3D computational tool which allows to study the impact of RMPs in ITER-like configurations [17, 18, 18]. It combines a Monte Carlos solver for fluid edge plasma transport (EMC3) and a Monte Carlo solver for kinetic transport of neutral gas (EIRENE). The former is based on a linearization of steady state particle, momentum and energy balance equations (see section A) which allows to calculate particle density, Mach number (i.e. flow velocity parallel to the magnetic field) and temperature for given transport coefficients such as the heat conductivity (although they depend on local plasma conditions). Therefore, a self consistent solution requires the iterative application of the transport solver.

Put in mathematical terms, the transport solver can be represented by the operator

$$\Phi : Y \mapsto X, \qquad X, Y \in \mathcal{P} \tag{1.1}$$

which maps the plasma state Y to the plasma state X ($\mathcal{P}$ denotes the abstract set of all plasma states). A self consistent solution X^* of the underlying physical model requires that

$$X^* = \Phi(X^*) \tag{1.2}$$

i.e. it requires that X^* is a fixed-point of Φ. The simulation procedure described above then formally represents a fixed-point iteration

$$X_{n+1} = \Phi(X_n) \tag{1.3}$$

based on an (within certain limits arbitrary) initial plasma state X_0. Convergence of a simulation run (i.e. of the sequence X_n) can be measured by the difference between iterations

$$\Delta_{n+1} \; = \; \|X_{n+1} \; - \; X_n\| \tag{1.4}$$

for some norm $\|.\|$ depending on the details of the plasma state representation. However, the convergence of the present solver is limited by the noise level intrinsic to Monte Carlo methods (i.e. Δ_n will at best saturate at a finite level δ_{MC}). A key factor for this noise level δ_{MC} is the number of Monte Carlo particles used in each simulation. So far, only a very basic assessment of the convergence of the sequence X_n for the present Monte Carlo fluid solver has been performed [19, 16]. In particular, the question whether X_n converges at all has not been addressed yet. Recent simulations which explore access to

detached plasma states have shown unstable behavior, i.e. densities and temperatures do not converge to a steady level. The present report is dedicated to exploring these issues.

An alternative approach to characterize the plasma boundary is the application of strongly simplified two-point models (sometimes referred to as *1/2-dimensional* models to account for the minimal spatial two point resultion and to distinguish from zero dimensional one-point models), e.g. the well established class of two-point model extensively explored in [20]). They allow a rather qualitative examination of the plasma boundary and are e.g. applied for an analysis of two dimensional [21] and three dimensional [22] numerical modeling. While it has already been used to evaluate physical aspects of simulation results, it is now used to study numerical features of the simulation procedure in order to study the stability of simulation results. The basic two-point model with a generic extension is revisited in section 2. A linearized version of this model is then derived in order to mimic the linearized transport solver EMC3 and its iterative application. It is demonstrated that even this simple model exhibits very complicated dynamics: a periodic doubling route to chaos which is similar to the one observed for the famous *Logistic map* [23]. Furthermore, wavelike oscillations which reflect the behavior of 3D simulations with EMC3-EIRENE are presented. The second part of this report is dedicated to the development of an adaptive relaxation scheme in section 3 which allows to suppress these oscillations. An implementation for 3D plasma edge transport simulations is presented and it is demonstrated that a stable solution can be found.

2. Two-point model analysis of iterated transport solvers

The two-point model (see section 5.2 and 5.4 in [20]) is a *1/2-dimensional* model for the plasma edge layer referred to as scrape-off layer (SOL). The SOL is the layer just outside the last closed magnetic flux surface (which holds the main plasma), thus comprising the region where magnetic field lines are diverted to intersect specific solid surfaces called divertor targets. These surfaces provide a sink for the plasma particles (which then recombine and re-enter the plasma as neutral particles, a process referred to as recycling), resulting in a rapid flow towards the divertor targets caused by particles which diffuse from the main plasma to the SOL. The so-called Bohm criterion indicates that the flow velocity increases to (and may exceed) sound speed at the target (or rather at the entrance to a thin sheath of net charge in front of the target). The intention of the two-point model is to relate plasma conditions between two locations:

upstream (index u): at the last closed flux surface halfway between targets (often approximated at the outer midplane of the torus for single-null configurations) and

downstream (index t): at the target

The main assumptions of the two-point model, which essentially allow to simplify the particle, parallel momentum and energy balance, are: high recycling conditions at the target. I.e. plasma particles are recycled in a thin layer in front of the target which is considered the only region with plasma flow, resulting in predominantly conductive heat transport (see section 5.2 in [20] for more details). The resulting model equations are:

$$2\, n_t\, T_t = f_{\mathrm{mom}}\, n_u\, T_u \tag{2.1}$$

$$T_u^{7/2} = T_t^{7/2} + \frac{7\, f_{\mathrm{cond}}\, q_\parallel\, L}{2\, \kappa_{0e}} \tag{2.2}$$

$$(1 - f_{\mathrm{power}})\, q_\parallel = \gamma\, e\, n_t\, T_t\, c_{st} \tag{2.3}$$

The upstream density $n_u\,[\mathrm{m}^{-3}]$ and the parallel component of the heat flux $q_\parallel\,[\mathrm{W\,m}^{-2}]$ are taken as control parameters; the SOL length $L\,[\mathrm{m}]$, the sheath heat transmission coefficient $\gamma \approx 7$ and $\kappa_{0e} \approx 2000$ are constant parameters. Dependent variables are the upstream temperature $T_u\,[\mathrm{eV}]$ and the downstream temperature and density $T_t\,[\mathrm{eV}]$ and $n_t\,[\mathrm{m}^{-3}]$, respectively. The sound speed at the target is given by $c_{st}\,[\mathrm{m\,s}^{-1}] = \sqrt{2\, e\, T_t/m}$.

A generic extension by correction factors $f_{\text{power}}, f_{\text{mom}}, f_{\text{cond}} \in [0,1]$ allows to include various processes which are neglected in the original basic two-point model:

- volumetric power losses due to radiation and charge exchange losses ($f_{\text{power}} > 0$)
- momentum losses due to the frictional collisions with neutrals, viscous forces and volume recombinations ($f_{\text{mom}} < 1$)
- finite contribution from heat convection ($f_{\text{cond}} < 1$)

An approximate solution can be derived for prescribed correction factors: for $T_u > T_t$ and due to the large exponents in (2.2) one finds:

$$T_u \approx \underbrace{\left(\frac{7\, q_\parallel\, L}{2\, \kappa_{0e}}\right)^{2/7}}_{=T_{u0}} f_{\text{cond}}^{2/7} \tag{2.4}$$

The downstream temperature T_t can be obtained by combinding (2.1) and (2.3) to eliminate n_t, which in turn can be derived from (2.1) with the previously calculated T_t:

$$T_t = \underbrace{\frac{m}{2\, e}\, \frac{4\, q_\parallel^2}{\gamma^2\, e^2\, n_u^2\, T_{u0}^2}}_{=F_u}\, \frac{(1-f_{\text{power}})^2}{f_{\text{mom}}^2\, f_{\text{cond}}^{4/7}} \tag{2.5}$$

$$n_t = \frac{f_{\text{mom}}\, n_u\, T_u}{2\, T_t} = \frac{n_u\, T_{u0}}{2\, F_u}\, \frac{f_{\text{mom}}^3\, f_{\text{cond}}^{6/7}}{(1-f_{\text{power}})^2} \tag{2.6}$$

2.1. Linearization

An alternative to the approximate solution of (2.1)-(2.3) is motivated by the approach used in edge transport codes. E.g. the EMC3 code is based on a linearization of the transport equations with prescribed transport coefficients (i.e. local sound speed and heat conductivity). A self-consistent solution then requires an iterative application, which is essentially a fixed-point iteration for some solver function Φ. In order to mimic the energy balance solver of the EMC3 code the following iterative scheme based on (2.2) and (2.3) is introduced:

$$T_{t,(n)} = \frac{(1-f_{\text{power}})\; q_\parallel}{\gamma\, e\, n_t \sqrt{\frac{2\, e}{m}}\, \sqrt{T_{t,(n-1)}}} \tag{2.7}$$

$$T_{u,(n)} = \frac{1}{T_{u,(n-1)}^{5/2}} \left[T_{t,(n-1)}^{5/2}\, T_{t,(n)} + \frac{7\, f_{\text{cond}}\, q_\parallel\, L}{2\, \kappa_{0e}} \right] \tag{2.8}$$

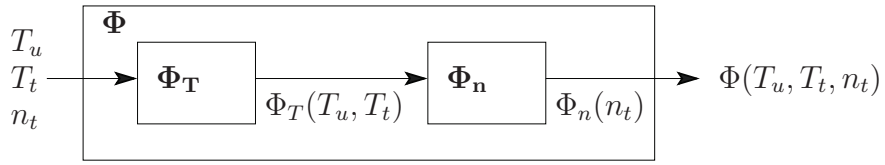

Figure 2.1.: Schematic representation a plasma solver Φ by the successive application of the operators Φ_T and Φ_n.

Furthermore, the particle and momentum balance solver of the EMC3 code can be represented by

$$n_{t,(n)} = \frac{f_{\text{mom}}\, n_u\, T_u}{2\, T_t}. \tag{2.9}$$

A relaxation scheme is applied to stabilize the iterative procedure. A single application of the energy balance solver (henceforth referred to as `ENERGY`) and the combined particle and momentum balance solver (henceforth referred to as `STREAMING`) can then be represented by the operators Φ_T and Φ_n, respectively:

$$\Phi_T : \begin{pmatrix} T_{u,(n-1)} \\ T_{t,(n-1)} \end{pmatrix} \mapsto \alpha \begin{pmatrix} T_{u,(n-1)} \\ T_{t,(n-1)} \end{pmatrix} + (1-\alpha) \begin{pmatrix} T_{u,(n)} \\ T_{t,(n)} \end{pmatrix} \tag{2.10}$$

$$\Phi_n : n_{t,(n-1)} \mapsto \alpha\, n_{t,(n-1)} + (1-\alpha)\, n_{t,(n)} \tag{2.11}$$

The parameter $\alpha \in [0, 1]$ is a prescribed relaxation factor which can be set individually for Φ_T and Φ_n. The operator Φ_T takes n_t as additional (unmodified) input and the operator Φ_n takes T_t and T_u as additional (unmodified) input. Let us define the plasma solver $\Phi(T_u, T_t, n_t)$ by the successive application of Φ_T and Φ_n (see figure 2.1). A solution to (2.1)-(2.3) is then given by the fixed-point(s) of Φ.

2.2. Convergence analysis

The convergence properties of the transport solver Φ are analysed in the following sections. The basic two-point model ($f_{\text{power}} = 0$, $f_{\text{cond}} = f_{\text{mom}} = 1$) is used for the first example, and afterwards an extension with n_t and T_t dependend correction factors is discussed.

2.2.1. Example 1: The basic two-point model

The control parameters $n_u = 4.2 \cdot 10^{19}\,\text{m}^{-3}$ and $q_{\parallel} = 0.8 \cdot 10^{-8}\,\text{W}\,\text{m}^{-2}$ are used for the following example and the SOL length is set to $L = 50\,\text{m}$. Initial conditions are

$n_{t,(0)} = n_u$ and $T_{t,(0)} = T_{u,(0)} = T_{u0}$ with T_{u0} from (2.4). The approximate solutions from (2.4)-(2.6) are:

$$T_u^* \approx 90.31\,\mathrm{eV}, \qquad T_t^* \approx 14.77\,\mathrm{eV}, \qquad n_t^* \approx 1.28 \cdot 10^{20}\,\mathrm{m}^{-3} \tag{2.12}$$

The evolution of the target temperature T_t using an iterative method is demonstrated in figure 2.2 (a). It can be seen that the iterative method converges only for relaxation factors $\alpha = 0.6$ and $\alpha = 0.8$, while oscillations occur for the smaller relaxation factors $\alpha = 0.2$ and $\alpha = 0.4$. The convergence rate depends on the level of relaxation, which is demonstrated in figure 2.2 (b) by the difference ΔT_t between two iteration steps normalized to the approximate solution T_t^*. It can be seen that machine precission ($\sim 10^{-16}$ for double precision) can be reached after slightly more than 200 iterations with $\alpha = 0.5$ while it takes about 700 iteration for $\alpha = 0.8$. Furthermore, it can be seen that the magnitude of the oscillations for $\alpha = 0.2$ and $\alpha = 0.4$ remains stable.

Such oscillatory behavior is a feature of non-linear maps, the Logistic map beeing a famous example [23]. This map exhibits a "period doubling route to chaos", i.e. the oscillation period doubles at certain values of a control parameter, turning to chaotic behavior at some point. A similar bifurcation diagram is indeed found for the present two-point edge plasma model as can be seen in figure 2.3 (a). The transition between convergence and oscillatory behavior occurs at $\alpha_0 \approx 0.43$ and at $\alpha_1 \approx 0.26$ the oscillation period jumps from 2 to 4 iterations. The bifurcation intervals become smaller and smaller for each period doubling and at $\alpha_\infty \approx 0.195$ a transition to chaotic behavior occurs. Let α_n denote the value at which the n-th period doubling takes place (i.e. when the period increases from 2^n to 2^{n+1}), then the ratio of each bifurcation interval to the next can be calculated for $n \geq 2$:

$$\delta_n = \frac{\alpha_{n-1} - \alpha_{n-2}}{\alpha_n - \alpha_{n-1}} \tag{2.13}$$

This ratio is shown by the blue line in figure 2.3 (b) up to the 10th period doubling. A feature of the Logistic maps is the limit

$$\delta_F = \lim_{n\to\infty} \delta_n = 4.669201609\ldots \tag{2.14}$$

This so-called Feigenbaum constant δ_F (indicated by the green line in figure 2.3 (b)) has been found to be universal for a large class of dynamical systems and it can also be observed for the two-point edge plasma model.

In order to account for the noise intrinsic to Monte Carlo methods, each of the linearized two-point model equations for $T_{t,(n)}$, $T_{u,(n)}$ and $n_{t,(n)}$ is multiplied by a noise factor f:

$$f = 1 + \beta\,\xi, \tag{2.15}$$

(a)

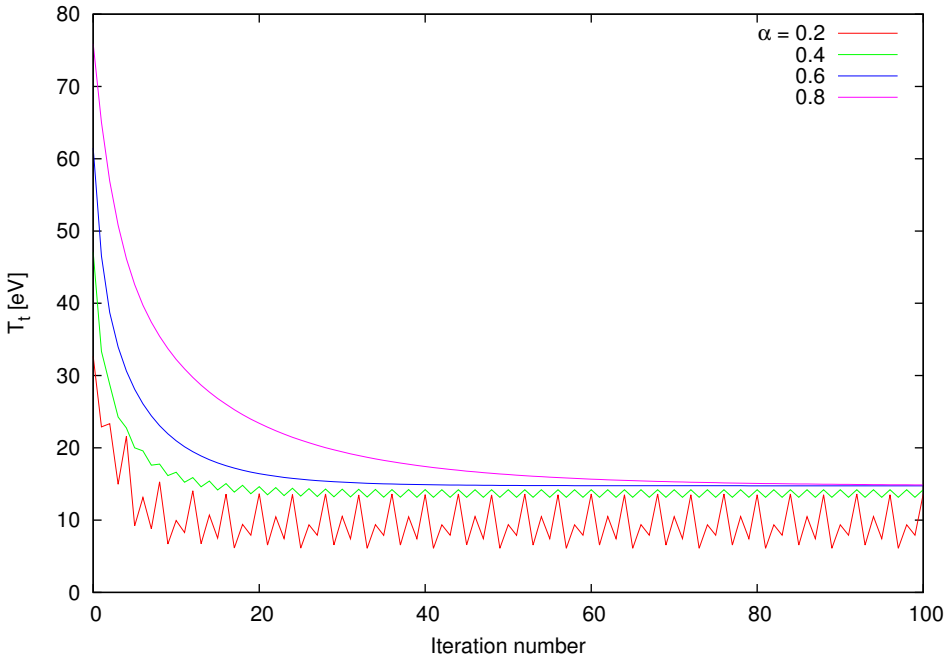

(b)

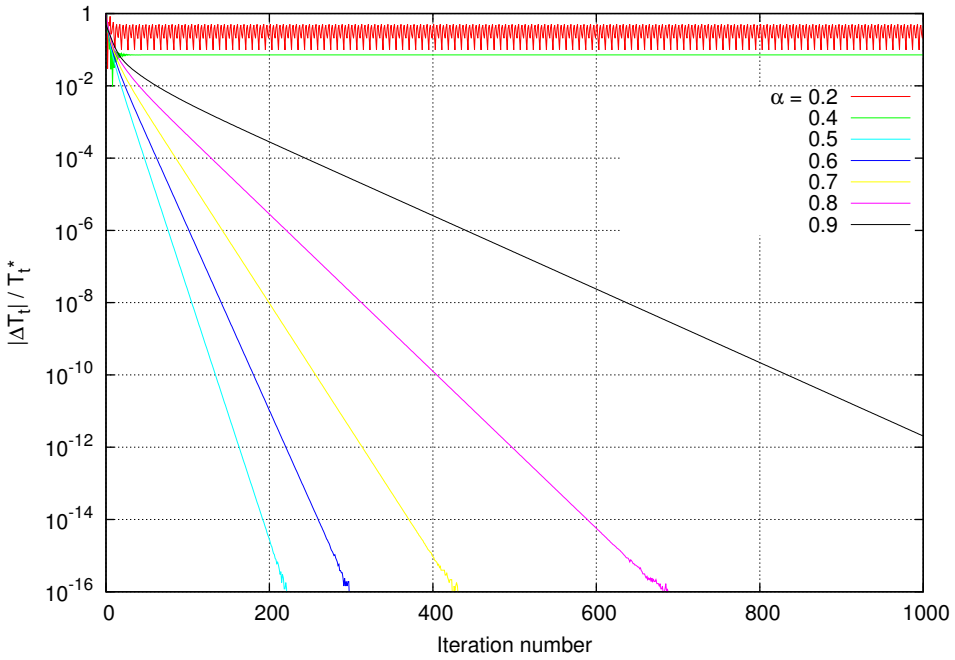

Figure 2.2.: (a) Iterated target temperature T_t and (b) the corresponding normalized differences between two iteration steps for different relaxation factors α.

(a)

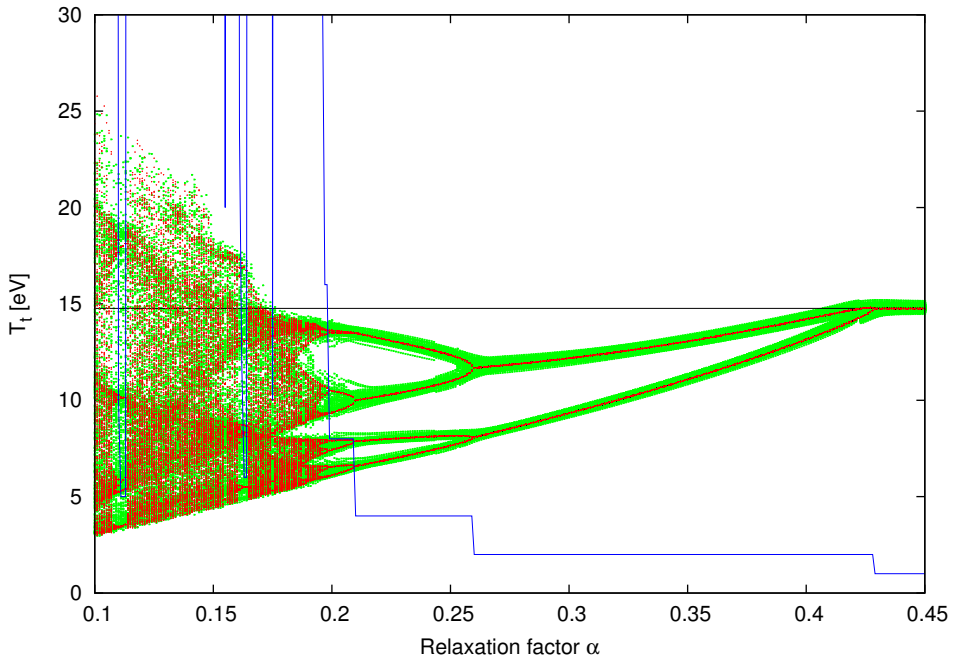

(b)

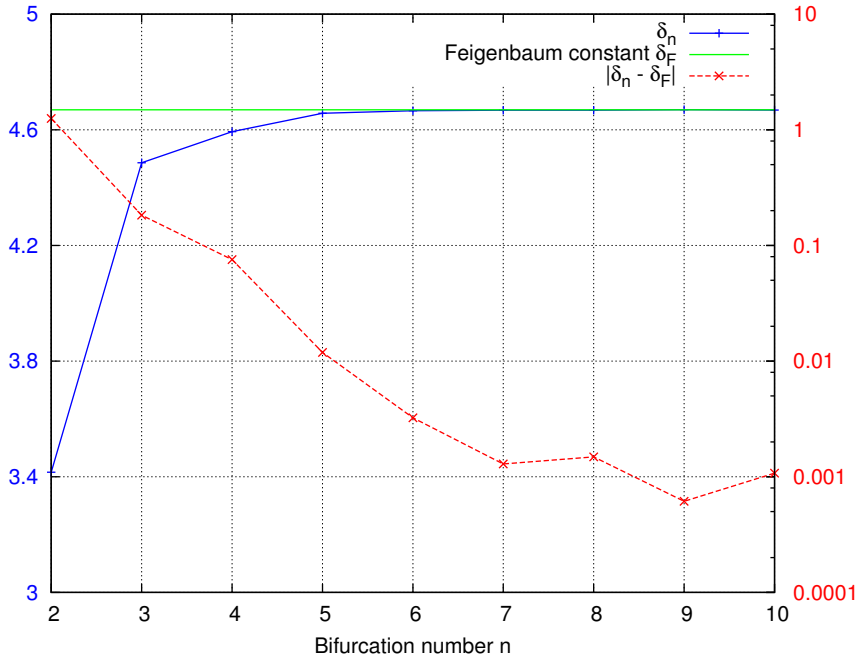

Figure 2.3.: (a) Final 256 of 8192 iterations of T_t: without noise (red) and with noise (green). The oscillation period is given in blue, T_t^* is indicated by the black line. (b) Ratio of bifurcation intervals δ_n and its deviation from the Feigenbaum constant δ_F.

where ξ is a distributed random variable and β determines the noise level. The resulting bifurcation diagram for $\beta = 1\,\%$ (green dots in figure 2.3 (a)) is similar to the one without noise.

2.2.2. Example 2: The extended two-point model

Of particular interest for magnetically confined fusion are low target temperatures, at which atomic processes (e.g. ionization and radiation) become very sensitive to the local temperature. Hence, a realistic extension of the basic two-point model requires correction factors which depend on plasma conditions. Power losses due to hydrogen recycling can be accounted for by

$$f_{\text{power}} = \frac{\varepsilon\,\Gamma_t}{q_{\parallel}} \tag{2.16}$$

based on the target flux $\Gamma_t = n_t\,c_{st}$ and the electron energy loss ε for one ionization event. The latter is given by the ionization energy $E_{\text{iz}} = 13.6\,\text{eV}$ and the rate coefficients for ionization $\langle\sigma_{\text{iz}}v\rangle$ and the respective radiation losses P_{rad} (which are both tabulated in n_t-T_t space and are taken from ADAS [24, 25] for the present example):

$$\varepsilon = \frac{E_{\text{iz}}\cdot\langle\sigma_{\text{iz}}v\rangle + P_{\text{rad}}}{\langle\sigma_{\text{iz}}v\rangle} \tag{2.17}$$

Rate coefficients $\langle\sigma_{\text{iz}}v\rangle$ and P_{rad} are shown in figure 2.4 (a), the resulting energy losses per ionization event are shown in figure 2.4 (b). Furthermore, the contribution from heat convection due to upstream sources is approximated as follows: an exponential ansatz $\exp(-x/\lambda)$ is assumed for the penetration of neutral particles with λ given by

$$\lambda = \frac{v_{th}}{n_t\,\langle\sigma_{\text{iz}}v\rangle}. \tag{2.18}$$

For a target plate temperature of 650 K and for deuterium: $v_{th} \approx 1.64\,\text{km}\,\text{s}^{-1}$. The fraction of neutral particles which penetrate beyond $x_0 = 0.004\,L$ (which is about one fourth of the SOL length at a field line inclination angle of 1 deg) is considered as upstream sources. The resulting correction factor is

$$f_{\text{cond}} = 1 - \exp(-x_0/\lambda) \tag{2.19}$$

which is shown in figure 2.5. Momentum losses for $T_t < T_c = 4\,\text{eV}$ are approximated by the simple (and rather arbitrary) ansatz

$$f_{\text{mom}} = 1 - \left(\frac{T_t - T_c}{T_c}\right)^2. \tag{2.20}$$

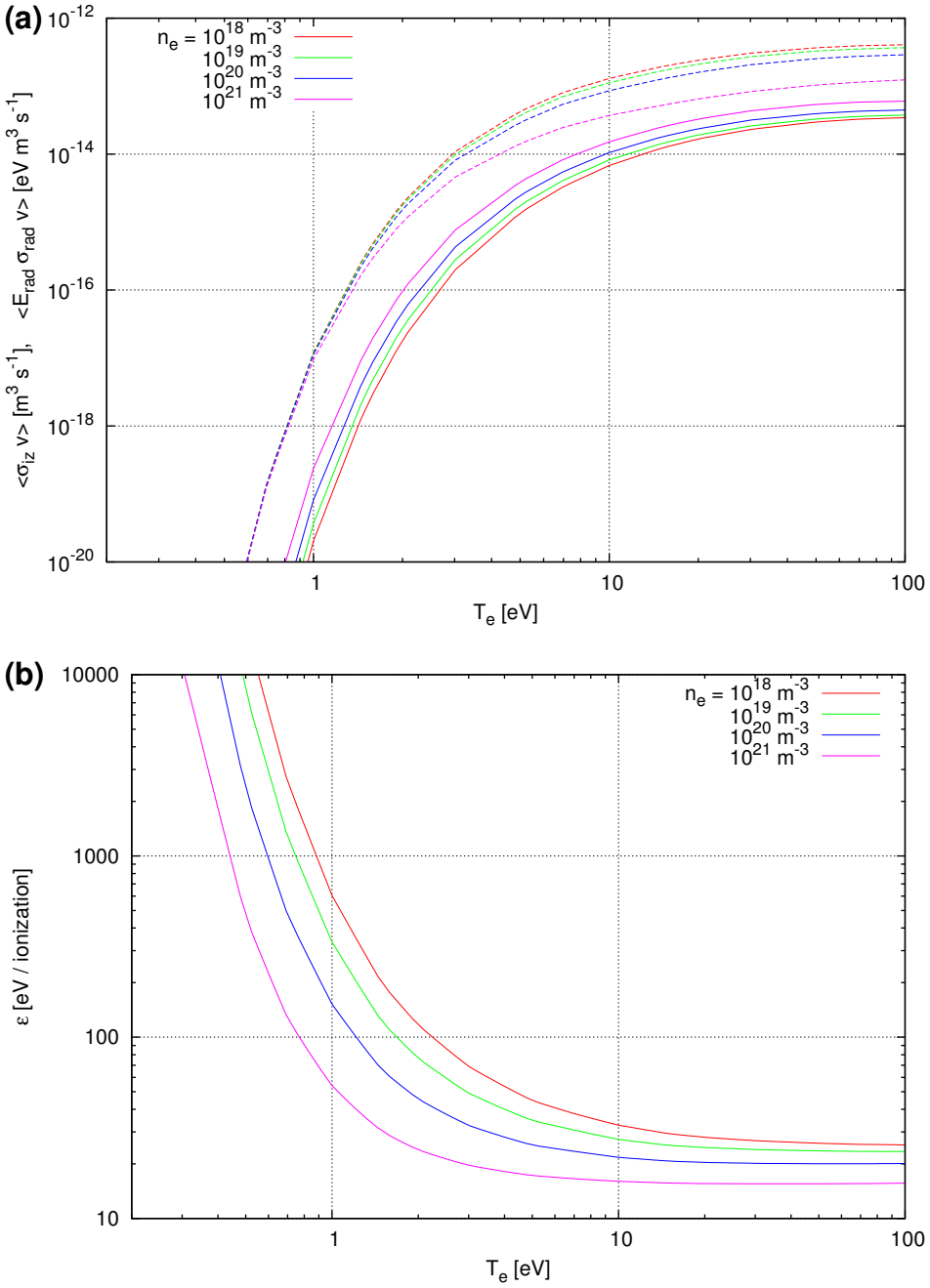

Figure 2.4.: (a) Rate coefficients for ionization ($\langle \sigma_{\mathrm{iz}} v \rangle$, solid lines) and for the corresponging energy losses due to radiation (P_{rad}, dashed lines). (b) The resulting energy losses ε per ionization event.

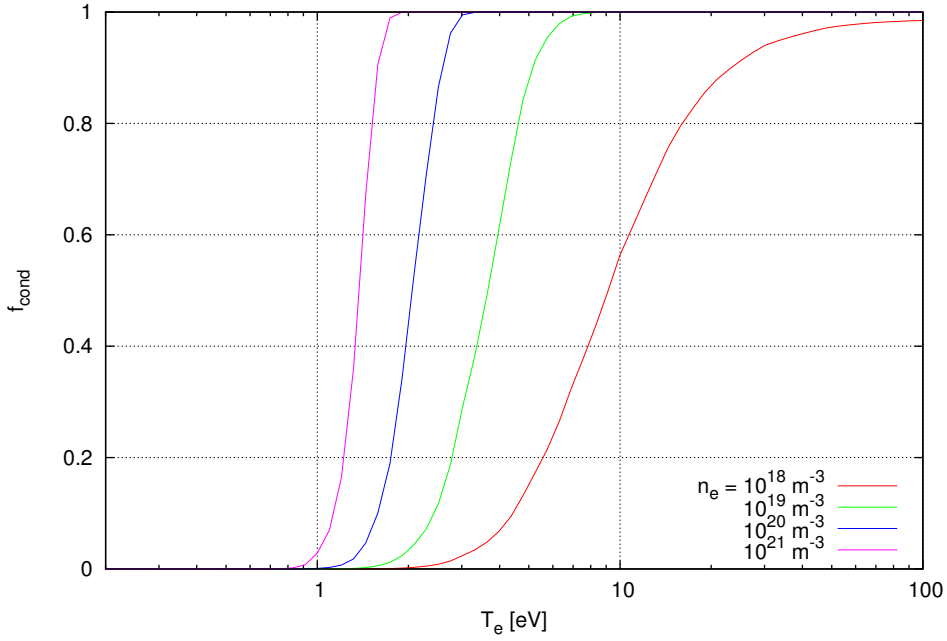

Figure 2.5.: Correction factor f_{cond} for a finite contribution of convective heat transport due to upstream sources.

While it was straightforward to find an (approximate) solution for the basic two-point model, an explicit solution for the extended two-point model can rarely be found due to the n_t and T_t dependence of f_{power}, f_{cond} and f_{mom}. However, at least a graphical solution can be found from (2.5) and (2.6) by solving each of the two equations for F_u. The n_t and T_t dependence of these two F_u versions is shown in figure 2.6 (a) and (b), respectively (note that F_u in figure 2.6 (b) depends on the control parameters n_u, $q_\parallel$ and L as well). Reference values for $n_u = 4.2 \cdot 10^{19}\,\mathrm{m}^{-3}$, $q_\parallel = 0.555 \cdot 10^{-8}\,\mathrm{W\,m}^{-2}$ and $L = 50\,\mathrm{m}$ are

$$T^*_{u0} \approx 81.35\,\mathrm{eV}, \qquad F^*_u \approx 8.76. \tag{2.21}$$

An overlay of the two contour lines $F_u(n_t, T_t) = F^*_u$ in figure 2.6 allows to estimate the solution to

$$T^*_t \approx 1.6\,\mathrm{eV}, \qquad n^*_t \approx 6.2 \cdot 10^{20}\,\mathrm{m}^{-3} \tag{2.22}$$

Although a unique solution exists for the present example, the iterated solver does not provide a stable solution. As can be seen in figure 2.7, continuous wavelike oscillations (unlike the discrete oscillations of the previous example) occur once T_t drops to the level of T^*_t. These waves cannot be suppressed by increasing the level of relaxation:

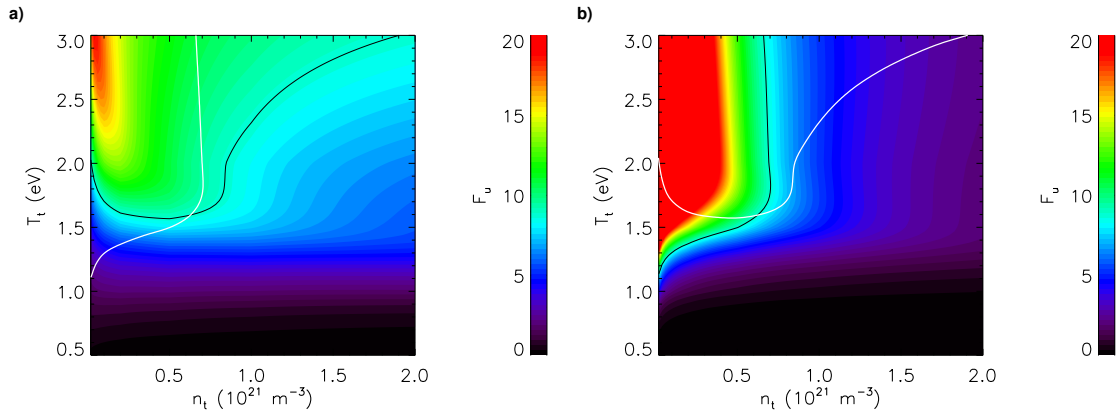

Figure 2.6.: (a) $F_u(n_t, T_t)$ according to (2.5), (b) the same for (2.6). The contour line $F_u(n_t, T_t) = F_u^*$ is given in black; the contour line of the opposite plot is given in white.

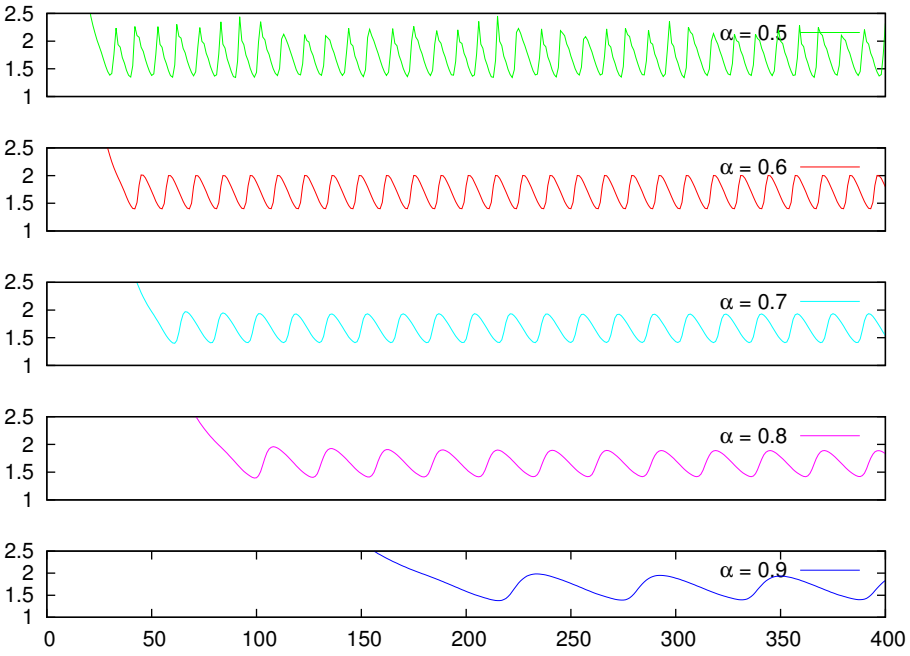

Figure 2.7.: Iterated target temperature T_t for different relaxation factors α. Initial conditions are $n_{t,(0)} = 10^{19}\,\mathrm{m}^{-3}$ and $T_{u,(0)} = T_{t,(0)} = 40\,\mathrm{eV}$.

(a)

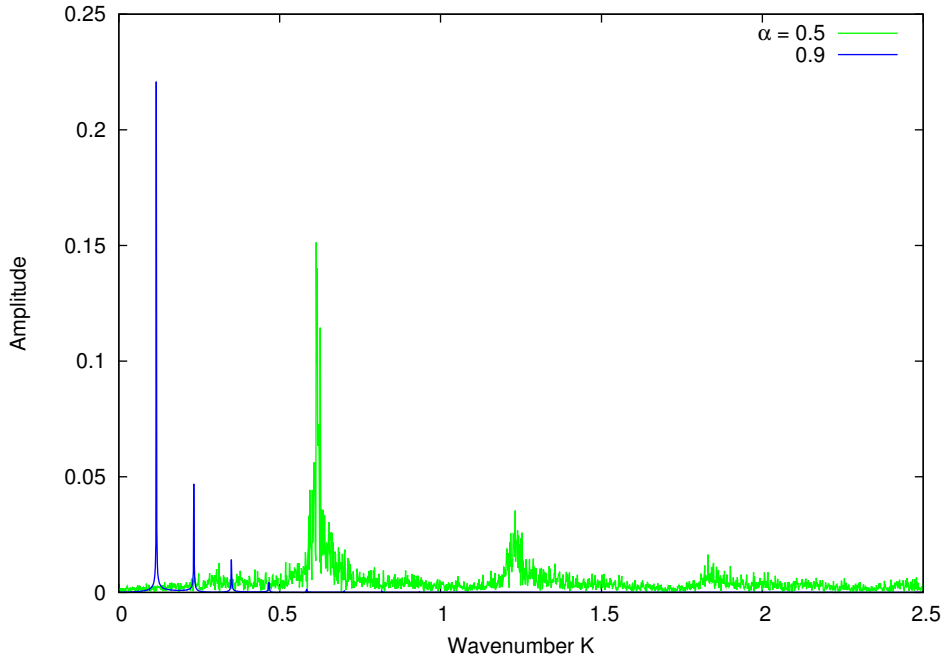

(b)

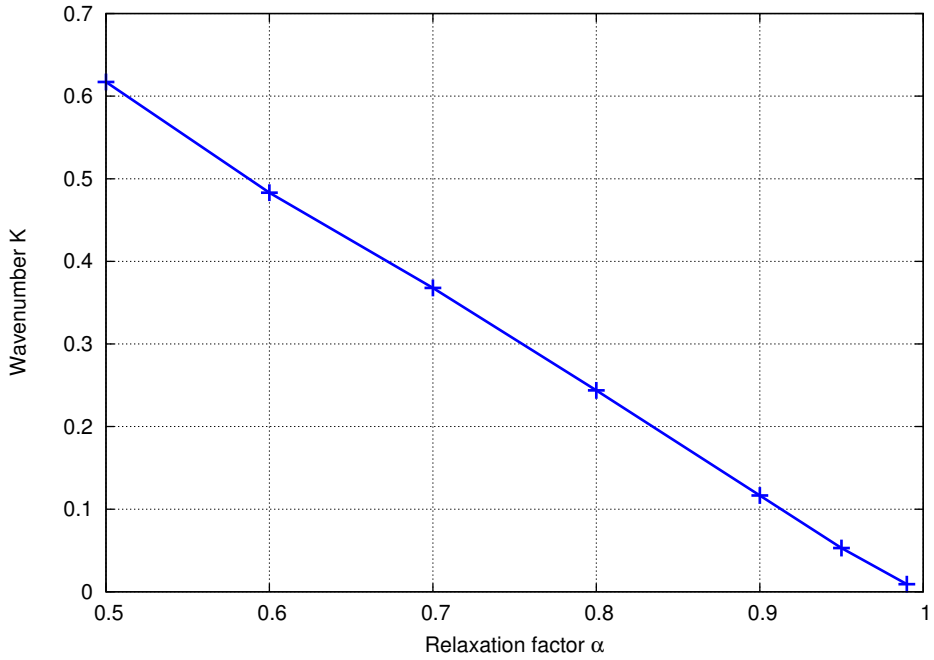

Figure 2.8.: (a) Fourier analysis of T_t using the second set of 4096 iterations. (b) Main wavenumber of the oscillations.

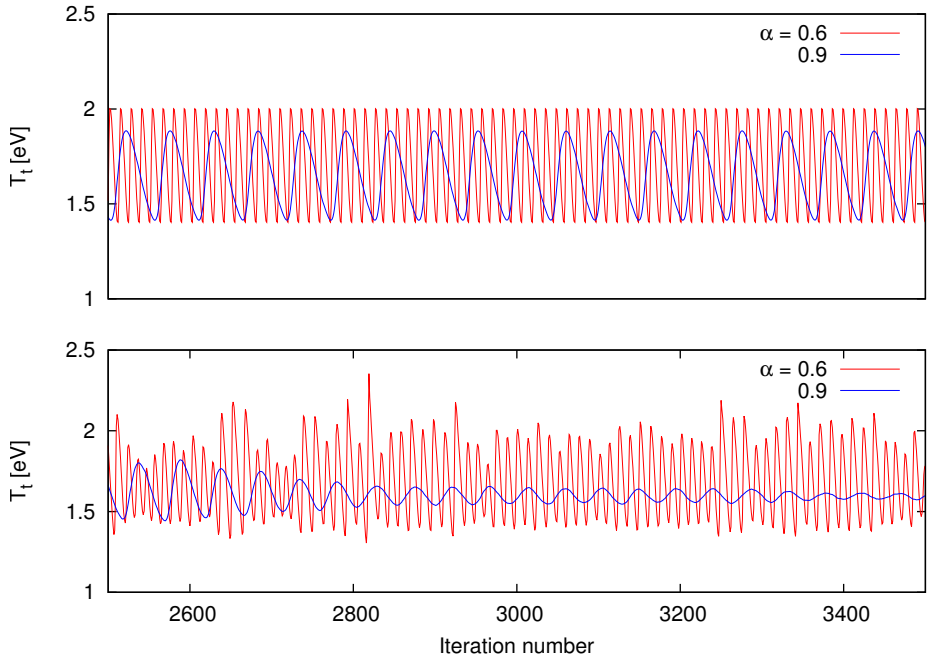

Figure 2.9.: Target temperature T_t after many iterations: without noise (upper part) and with noise (lower part).

the amplitude remains unaffected but the wavelength Λ increases with increasing α (see also upper part in figure 2.9). A Fourier analysis (figure 2.8 (a)) allows to extract the correspondig wavenumber $K = 2\,\pi/\Lambda$ which is shown in figure 2.8 (b). It can be seen that $K \to 0$ for $\alpha \to 1$, i.e. the wavelength increases to infinity. The presence of noise, however, can lead to a reduction of the amplitude, but only for strong relaxation and many iterations (see lower part of figure 2.9). The same noise model as in the previous example has been used here. It can be seen that it takes about 3000 iterations for the amplitude to noticably decrease which would be unpractical in applications of more sophisticated transport solvers.

2.2.3. Implications for 2D/3D simulations

While the previous examples are of a rather academic nature, they nevertheless demonstrate what kind of behavior might occur in more elaborate edge transport models. The phenomenon of an oscillating target temperature is now investigated under more realistic conditions: the EMC3-EIRENE code is applied to an axisymmetric configuration at the DIII-D tokamak. The average target temperature T_{ISP} at the inner strike point of the magnetic separatrix is now taken as parameter of interest. The evolution of T_{ISP} is shown in figure 2.10, starting with $\alpha = 0.4$ (red) for 32 iterations. It can be seen that wavelike oscillations can indeed occur in state of the art edge transport simulations (see

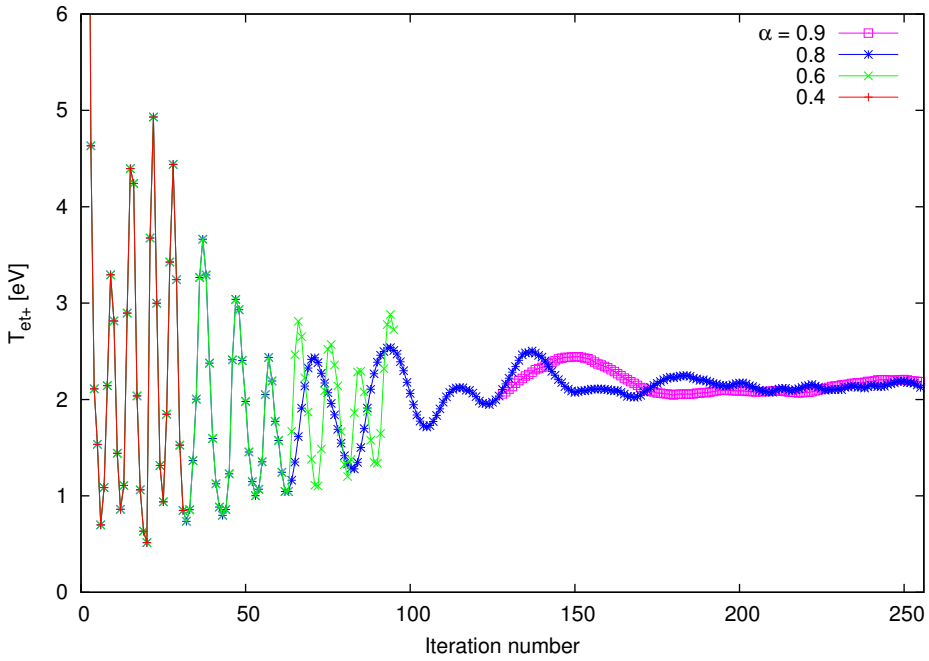

Figure 2.10.: Iterated target temperature T_{ISP} using the EMC3-EIRENE code for an axisymmetric configuration at the DIII-D tokamak.

also figure A.1). Increasing the relaxation factor to $\alpha = 0.6$ (green) allows to decrease the magnitude of the oscillations, however, the wavelength increases in return and a stable solution is not yet obtained. The relaxation factor is increased to $\alpha = 0.8$ after another 32 iterations, increasing yet again the wavelength of the oscillations. A rather stable solution can be obtained with $\alpha = 0.8$ and $\alpha = 0.9$, however, at the price that many iterations are required. This can be unpractical for big 3D simulations of RMP configurations which require an enormous amount of computational resources. Hence, an adaptive relaxation scheme which allows to adjust the level of relaxation for each iteration step might prove useful. This is the topic of the next chapter.

3. Convergence control by adaptive relaxation

The idea of an adaptive relaxation scheme is to adjust the level of relaxation in a way that allows a fast and stable convergence, i.e. it should allow a fast approach to the fixed-point without turning to an oscillatory state. A generic definition of a relaxation factor for iteration n is:

$$\alpha_n = \begin{cases} \alpha_{\text{weak}}, & \text{far from fixed-point} \\ \alpha_{\text{strong}}, & \text{when oscillations occur} \end{cases} \tag{3.1}$$

with $\alpha_{\text{weak}} \ll \alpha_{\text{strong}}$. Such a scheme is developed in the following sections.

3.1. Control scheme for discrete oscillations

A straightforward way to detect discrete oscillations of some plasma quantity Q is to look at the changes between iterations. Let $\Delta_{Q,(n)} = Q_{n-1} - Q_n$ denote the difference between iterations n and $n-1$, then the adapted relaxation factor for the n-th iteration can be defined as:

$$\alpha_{Q,n} = \begin{cases} \alpha_{\text{weak}}, & \Delta_{Q,(n-1)} \cdot \Delta_{Q,(n)} \geq 0 \\ \alpha_{\text{strong}}, & \text{else} \end{cases} \tag{3.2}$$

This relaxation scheme is applied to $Q = T_u, T_t, n_t$ of the basic two-point model example in section 2.2.1 when noise is present. The resulting evolution of T_t is shown in figure 3.1 for several values for α_{weak} while $\alpha_{\text{strong}} = 0.8$. It can be seen that this scheme allows a fast convergence for $\alpha_{\text{weak}} = 0.1 - 0.4$ while (discrete) oscillations are indeed suppressed. However, a more elaborate relaxation scheme needs to be developed to account for the continuous wavelike oscillations of the second example which have also been found in some simulations.

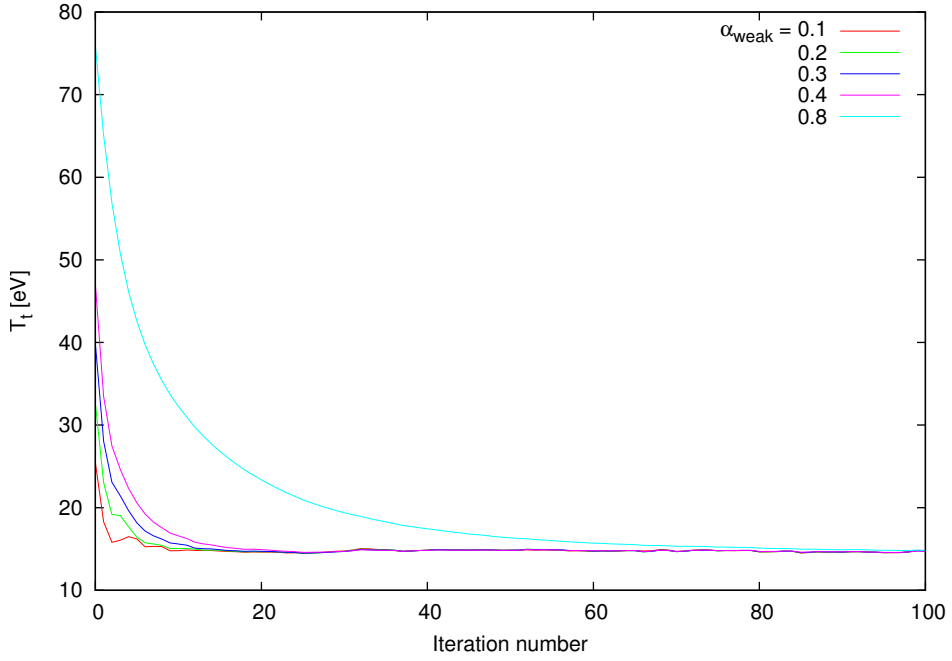

Figure 3.1.: Iterated target temperature T_t of the basic two-point model with noise (example 1) when the adaptive relaxation scheme (3.2) is applied.

3.2. Control scheme for continuous oscillations

In the following an adaptive relaxation scheme for simulations with the EMC3-EIRENE code is proposed. The target averaged electron and ion temperatures ($\overline{T}_{et}$, $\overline{T}_{it}$) are used as test quantities for the `ENERGY`-solver in the EMC3 code. Furthermore, the target averaged density $\overline{n}_t$ is used as test quantity for the `STREAMING`-solver and the total hydrogen recycling flux Γ_{rec} is used as test quantity for the `NEUTRAL`-solver (which is provided by the coupling to the EIRENE code for sources due to interactions between plasma and neutral gas). After each application of one of the above solvers, the sequence of the respective test quantity Q is post-processed to obtain the reference quantities $Q_{\max}$ and $Q_{\min}$. Either the last occurence of extremal values can be used to obtain $Q_{\max}$ and $Q_{\min}$ or all occurences can be taken into account by averaging. Both approaches are investigated below. If $Q_{\min} \lesssim Q \lesssim Q_{\max}$, then oscillatory behavior is assumed and strong relaxation should be applied. Otherwise it is assumed that the iterative solver is far from its fixed-point, and therefore a weak relaxation should be applied to allow fast convergence. Selected kernel functions which provide $\alpha(Q)$ are summarized in figure 3.2, showing a discrete (red) or smooth ($-x^2$-like, green and $\exp(-x^2)$-like, blue) transition between weak and strong relaxation.

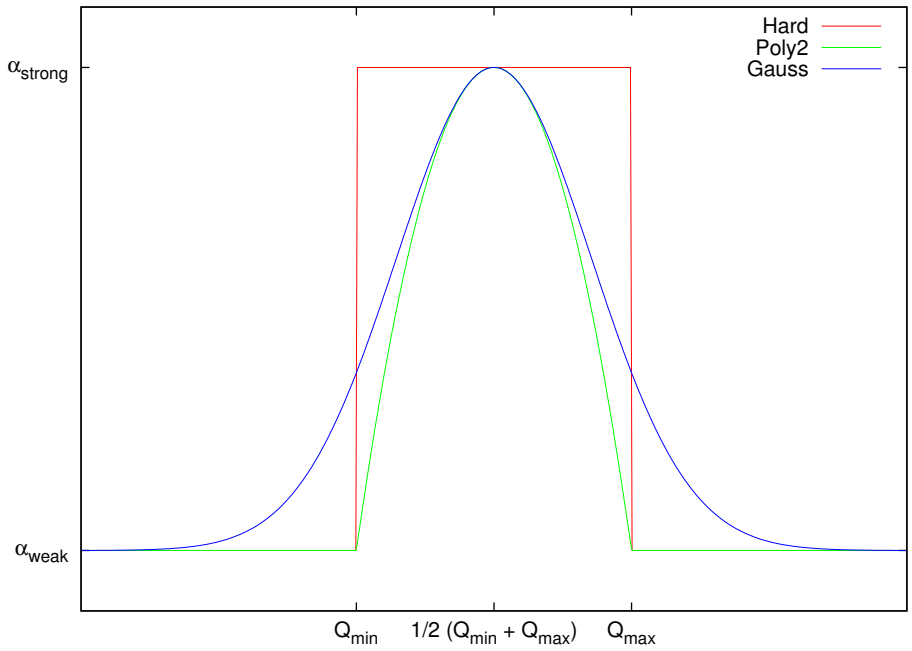

Figure 3.2.: Selected kernel functions for adaptive relaxation.

3.2.1. Last occurence of extremal values

Taking the last occurence of extremal values as reference, it is demonstrated in figure 3.3 that oscillatory behavior can be suppressed with this method (note that the presented $\overline{T}_{et}$ is averaged over both targets while T_{ISP} in figure 2.10 is the average over the inner strike point region only). A weak relaxation level of $\alpha_{\mathrm{weak}} = 0.4$ and a strong relaxation level of $\alpha_{\mathrm{strong}} = 0.9$ has been used. A steady state solution is reached at 50-60 iterations with the Hard- and Gauss-kernels while it takes some more iterations with the Poly2-kernel. This is much faster than if a high level of relaxation is used from the beginning, i.e. $\alpha = 0.9$ does not provide convergence after 160 iterations as shown by the magenty line in figure 3.3.

3.2.2. Averaging of extremal values

An alternative approach is to scan the test quantity sequence and calculate the averages of the local maxima $\overline{Q}_{\mathrm{max}}$ and minima $\overline{Q}_{\mathrm{min}}$ instead of using just the last ones, which might prove more stable once the intrinsic noise level is reached. The following analysis is based on the Gaussian kernel for α. As can be seen in the first row of figure 3.4, however, there is no significant difference to the previous method for $\alpha_{\mathrm{weak}} = 0.4$ and $\alpha_{\mathrm{strong}} = 0.9$, only that the relaxation stays at $\alpha \approx \alpha_{\mathrm{weak}}$ after about 30-35 iterations. Reducing α_{weak} to 0.1 results in one spike at the beginning and consequently results in

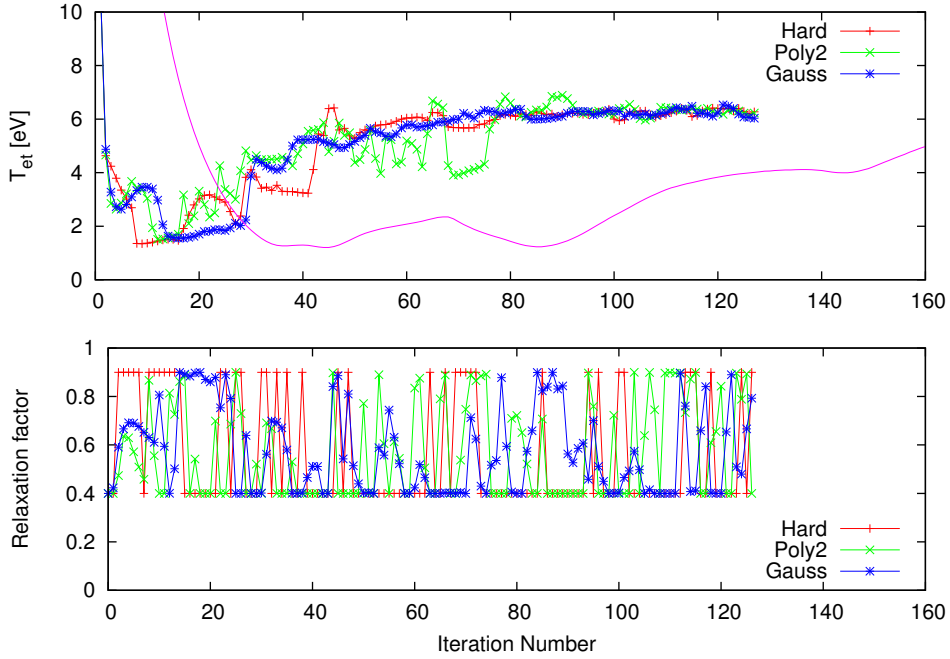

Figure 3.3.: Iterated electron target temperature $\overline{T}_{et}$ and the corresponding adaptive relaxation factor based on the last minimum and maximum of the sequence. The kernel function from figure 3.2 are applied to $\alpha_{\text{weak}} = 0.4$ and $\alpha_{\text{strong}} = 0.9$. The reference $\overline{T}_{et}$ for throughout strong relaxation at $\alpha = 0.9$ is given by the magenta line.

a larger $\overline{Q}_{\max}$. This in turn results in weak relaxation during the first 20 iterations. Afterwards, the level of relaxation increases and remains at a large level after another 20 iterations. As a results, the $\overline{T}_{et}$ sequence is less noisy than in the previous case.

While $\alpha_{\text{weak}} = 0.1$ is already quite low, it can be seen in the third row of figure 3.4 that some low level of relaxation must remain, i.e $\alpha_{\text{weak}} = 0$ does not provide a stable solution. An overview of the other test quantities $\overline{T}_{it}$, $\overline{n}_t$ and Γ_{rec} is given in figures 3.5, 3.6 and 3.7, respectively.

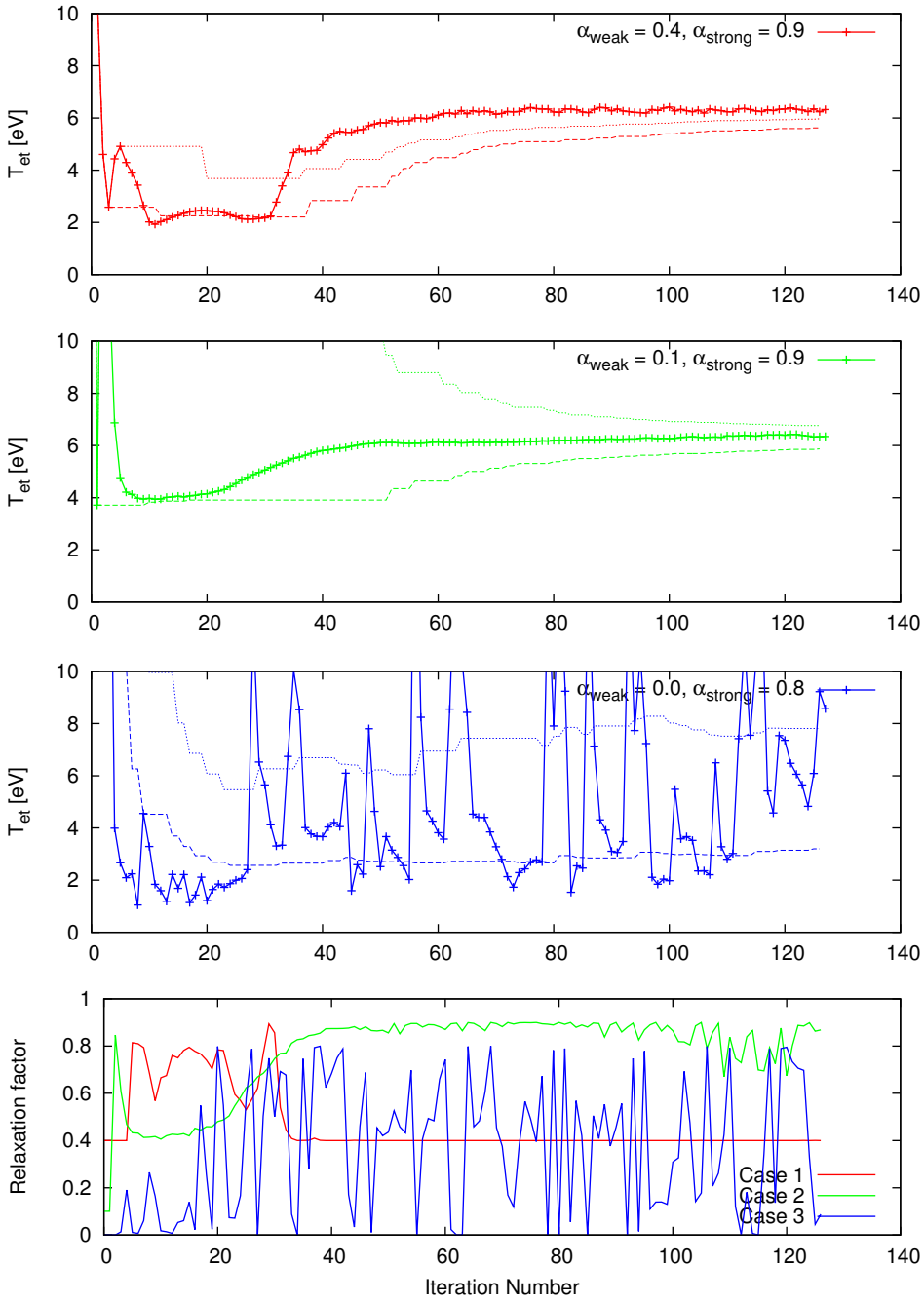

Figure 3.4.: Iterated electron target temperature $\overline{T}_{et}$ (solid line) for three cases and the corresponding adaptive relaxation factors based on the average maximum and minimum of the sequence. The latter are indicated by the dotted ($\overline{Q}_{\max}$) and dashed ($\overline{Q}_{\min}$) lines.

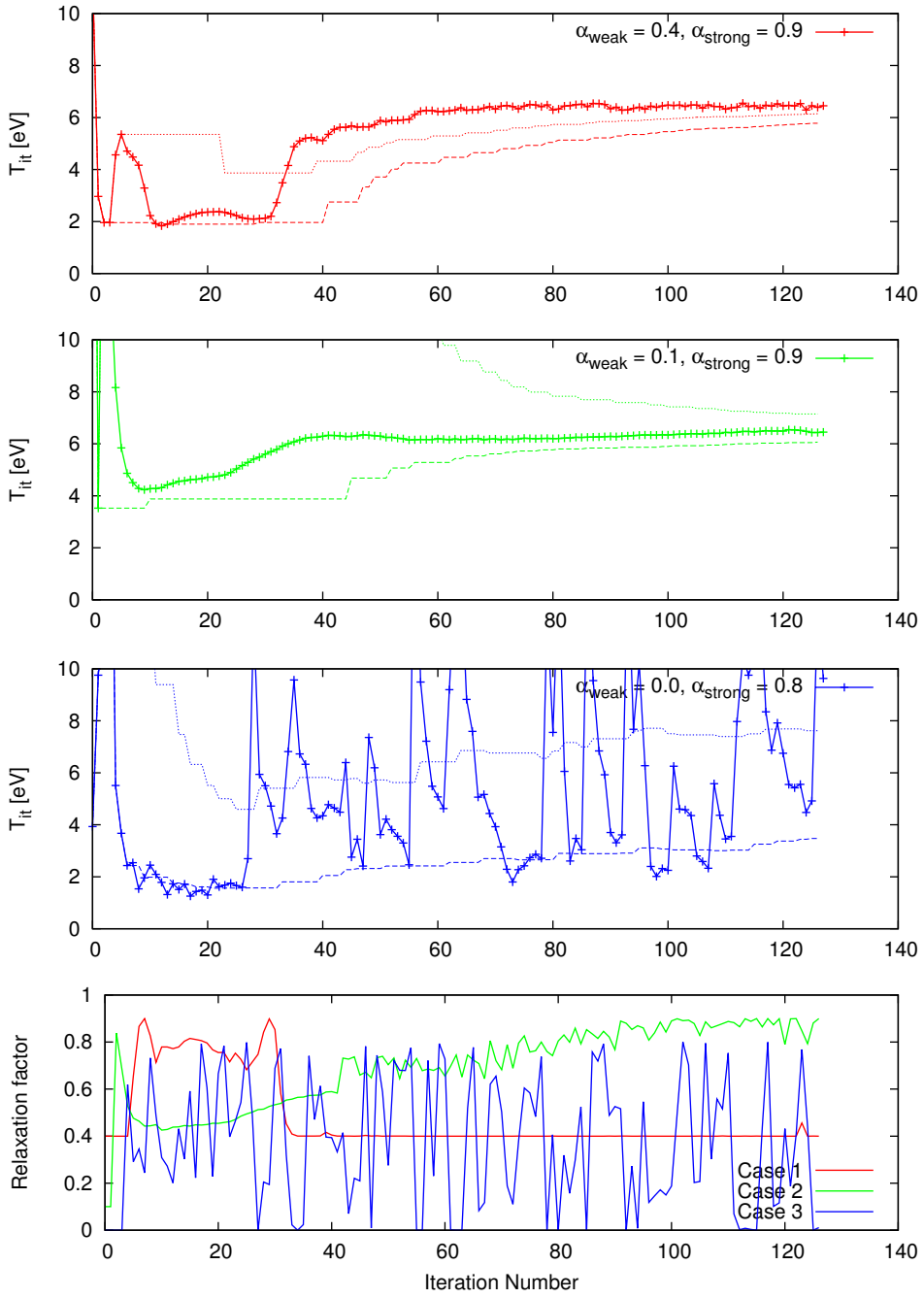

Figure 3.5.: Iterated ion target temperature $\overline{T}_{it}$ (solid line) for three cases and the corresponding adaptive relaxation factors based on the average maximum and minimum of the sequence. The latter are indicated by the dotted ($\overline{Q}_{\max}$) and dashed ($\overline{Q}_{\min}$) lines.

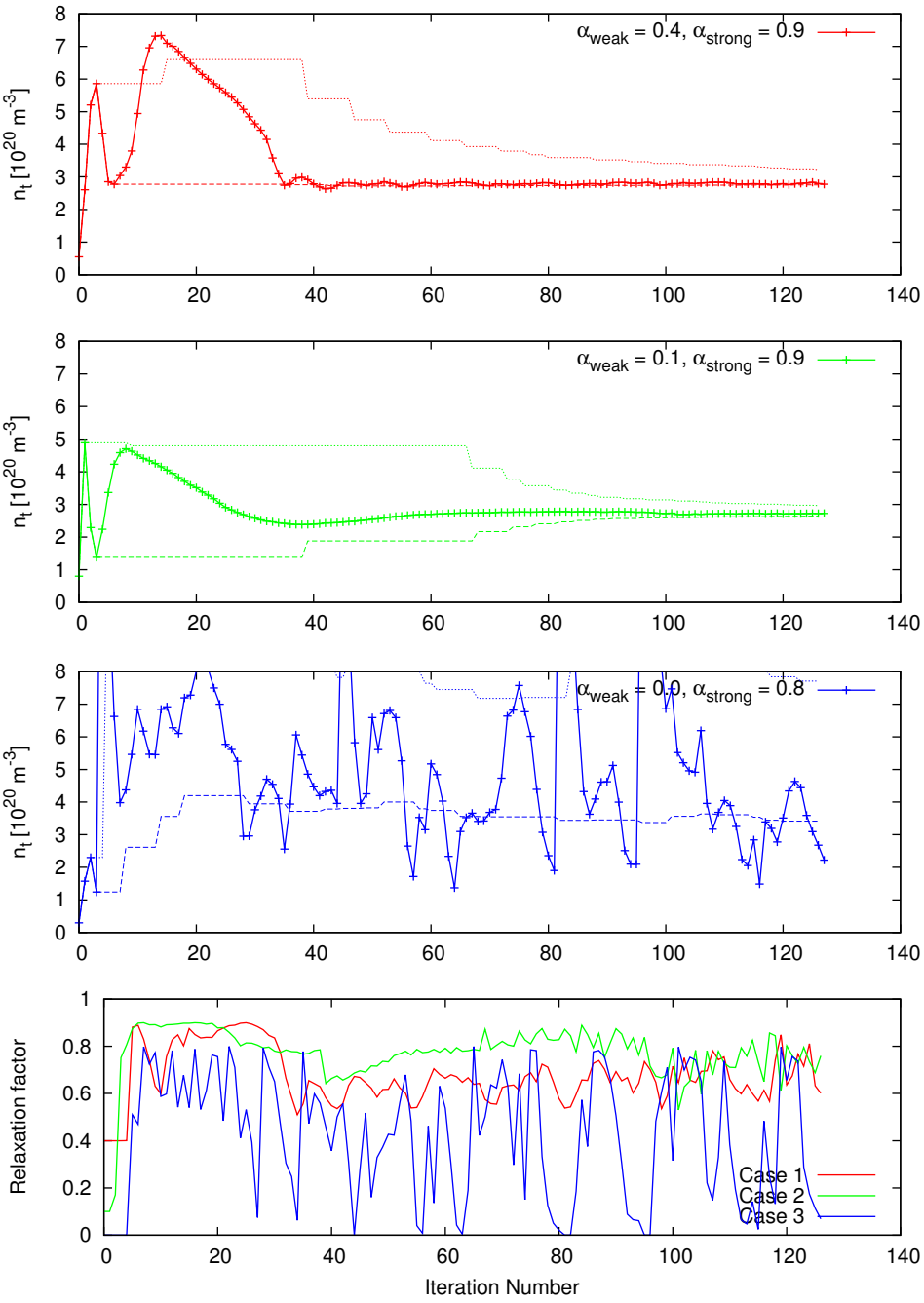

Figure 3.6.: Iterated target density $\overline{n}_t$ (solid line) for three cases and the corresponding adaptive relaxation factors based on the average maximum and minimum of the sequence. The latter are indicated by the dotted ($\overline{Q}_{\max}$) and dashed ($\overline{Q}_{\min}$) lines.

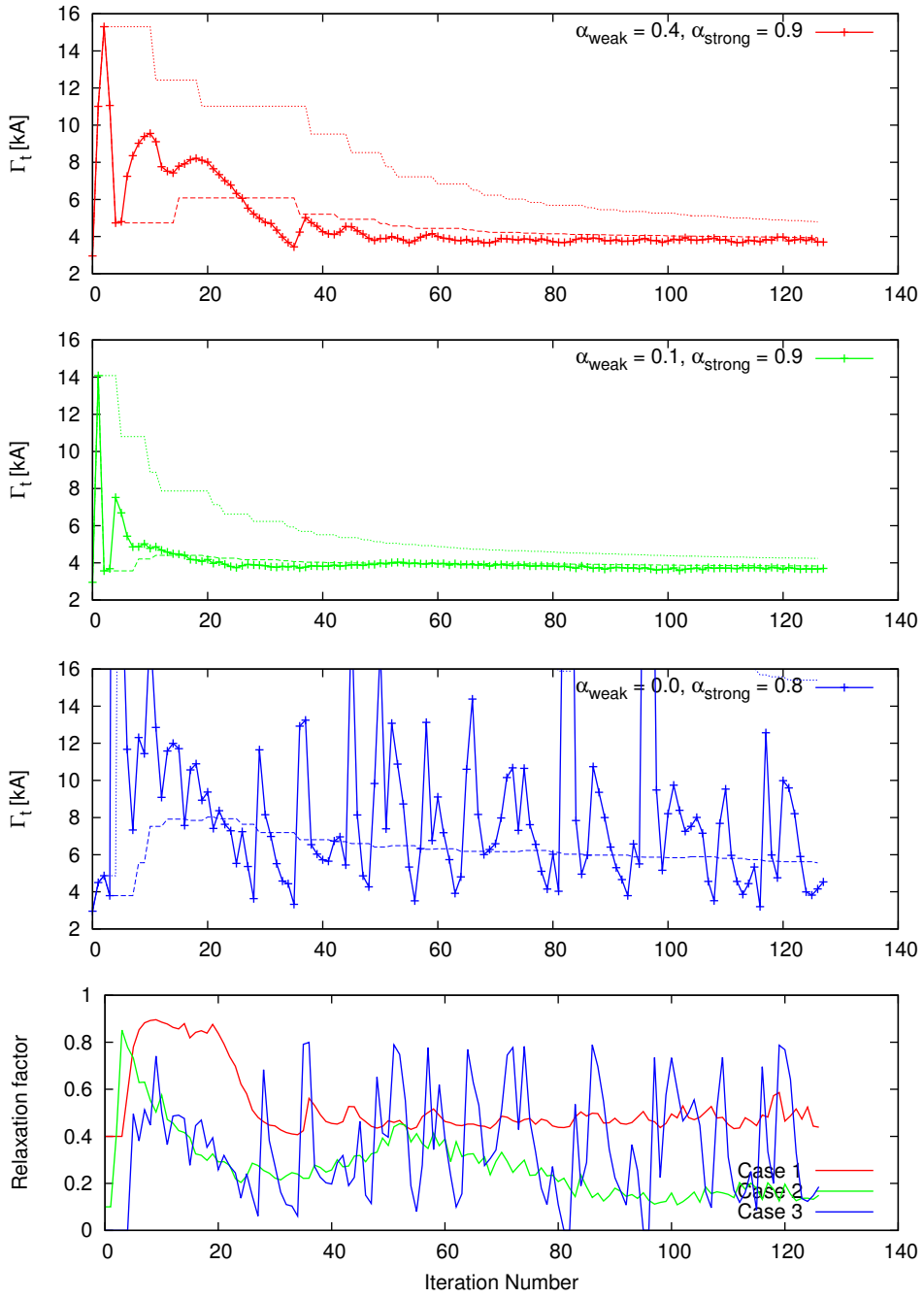

Figure 3.7.: Iterated total recycling flux Γ_{rec} (solid line) for three cases and the corresponding adaptive relaxation factors based on the average maximum and minimum of the sequence. The latter are indicated by the dotted ($\overline{Q}_{\mathrm{max}}$) and dashed ($\overline{Q}_{\mathrm{min}}$) lines.

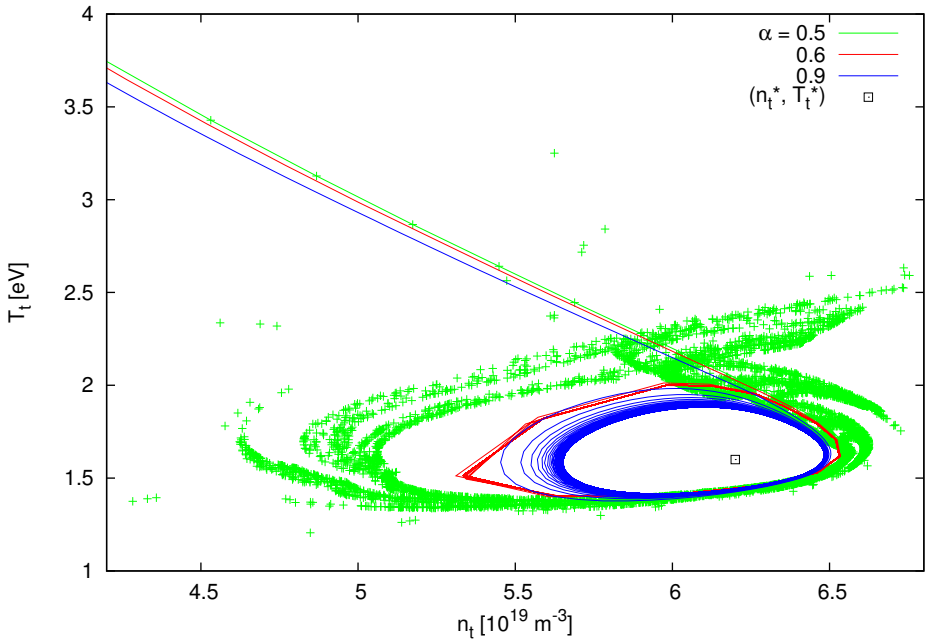

Figure 3.8.: The iterated two-point model in n_t-T_t space (for $\alpha = 0.5$ only the first 32 iterations are linkes by lines).

3.3. Outlook to further advancements

Implementing an adaptive relaxation scheme into 3D edge plasma simulations leaves plenty of room for optimizations. Let's go back to second example of the previous chapter, i.e. the extended two-point model, and take a closer look at the wavelike oscillations. The iterated plasma states are now shown in n_t-T_t space in figure 3.8. It can be seen that the plasma states are attracted to a circular orbit around the expected solution (n_t^*, T_t^*). Therefore, instead of applying an independent relaxation factor for n_t and T_t (and T_u), an integrated approach should be performed. The following post-processing analysis (which is easy to implement in the EMC3-EIRENE simulation scheme) is performed after each application of the transport solver Φ: The average extremal values $n_{t,\max}$, $n_{t,\min}$, $T_{t,\max}$ and $T_{t,\min}$ are calculated as before. If $n_{t,\max} > n_{t,\min}$ and $T_{t,\max} > T_{t,\min}$, i.e. after the first occurrence of a local extremum, then these are used to calculate the central values

$$n_c = \frac{n_{t,\max} + n_{t,\min}}{2}, \qquad T_c = \frac{T_{t,\max} + T_{t,\min}}{2} \tag{3.3}$$

and the normalized differences

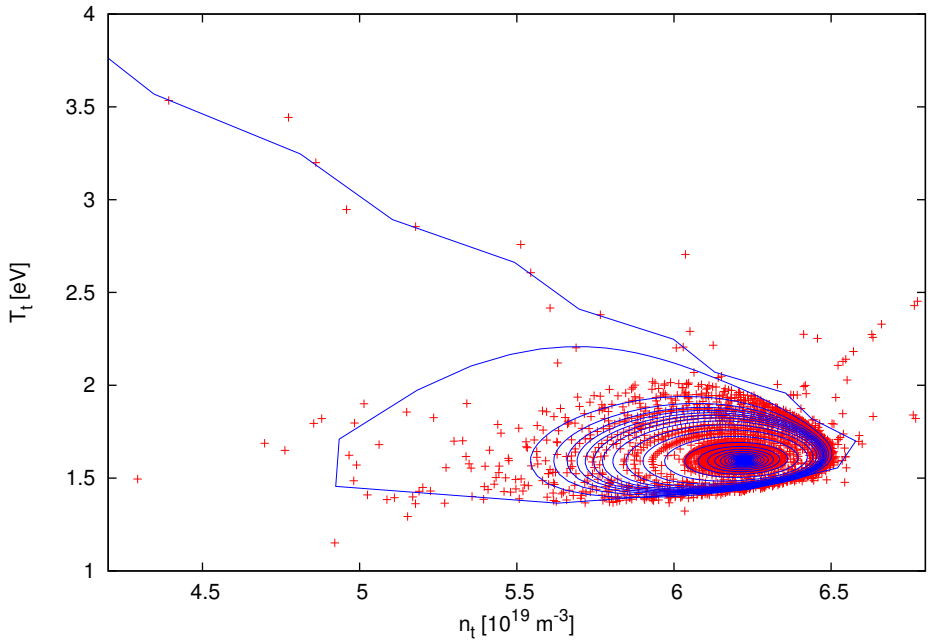

Figure 3.9.: The iterated two-point model in n_t-T_t space when adaptive relaxation based on (3.5) is applied: without noise (blue) and with noise (red).

$$\eta_n = \frac{n_{t,(n)} - n_c}{n_{t,\max} - n_{t,\min}}, \qquad \xi_n = \frac{T_{t,(n)} - T_c}{T_{t,\max} - T_{t,\min}}. \tag{3.4}$$

Contrary to the approach of the previous section, the adaptive relaxation factor now depends on the history of both n_t and T_t. A generalization of the Gaussian kernel is

$$\alpha_{n+1} = \alpha_{\text{weak}} + (\alpha_{\text{strong}} - \alpha_{\text{weak}}) \exp\left(-\eta_n^2 - \xi_n^2\right) \tag{3.5}$$

which is applied to both n_t and T_t after the next application of the solver (i.e. the $n+1$-th iteration). Setting $\alpha_{\text{weak}} = 0.45$ (which is above the limit for discrete oscillations) and $\alpha_{\text{strong}} = 0.99$, it can be seen in figure 3.9 that the circular orbit is destabilized and approaches the expected solution. However, convergence is very slow and noise can result in spontaneous excursions.

A better approach is motivated by the general character of a n_t-T_t cycle sketched in figure 3.10. In quadrant 1 the temperature approaches the central value, but the density exceeds the central value and continues to increase. Therefore, weak relaxation should be applied to T_t to allow a fast approach to the central values, and strong relaxation should be applied to n_t in order to slow down its overshoot. A basic filter for n_t which accounts

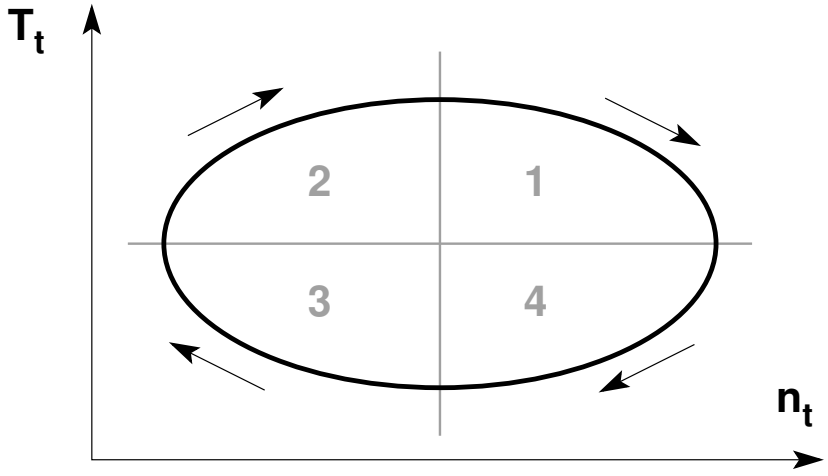

Figure 3.10.: Sketch of cycle in n_t-T_t space.

for these properties is shown by the black line in figure 3.11. A smoother version (green line) is given by

$$F(\eta, \xi) = \frac{1}{2} \left(1 + \sin\left(2\,\varphi\right)\right), \qquad \varphi = \arctan\left(\xi, \eta\right). \tag{3.6}$$

This filter allows to define the amount of relaxation for n_t:

$$\alpha_{n+1} = \alpha_{\text{weak}} + \left(\alpha_{\text{strong}} - \alpha_{\text{weak}}\right) F(\eta_n, \xi_n). \tag{3.7}$$

The corresponding relaxation factor for T_t is given by a phase shift of $\pi/2$. Much faster convergence can be obtained with this scheme, as demonstrated in figure 3.12. Furthermore, it can be seen that the performance of this relaxation scheme is also good in the presence of noise. Therefore, an implementation for 3D simulation is recommended. Such an implementation can also account for different behavior at inner (forward) and outer (backward) strike points (e.g. in semi-detached configurations) by evaluation two relaxation factors α_{ISP} and α_{OSP}. A smooth transition

$$\alpha(M) = \alpha_{\text{ISP}} \frac{1 + M}{2} + \alpha_{\text{OSP}} \frac{1 - M}{2} \tag{3.8}$$

is guided by the Mach number $M \in [-1, 1]$ and allows to avoid spatial discontinuities. An alternative approach is a transition guided by the underlying magnetic geometry, i.e. the forward (L_+) and backward (L_-) field line connection length to the divertor targets. The numerical calculation of the connection length by field line tracing provides $L_+ = L_- = L_{\text{cut}}$ in the confined region, and consequently an equally weighted average between α_{ISP} and α_{OSP}.

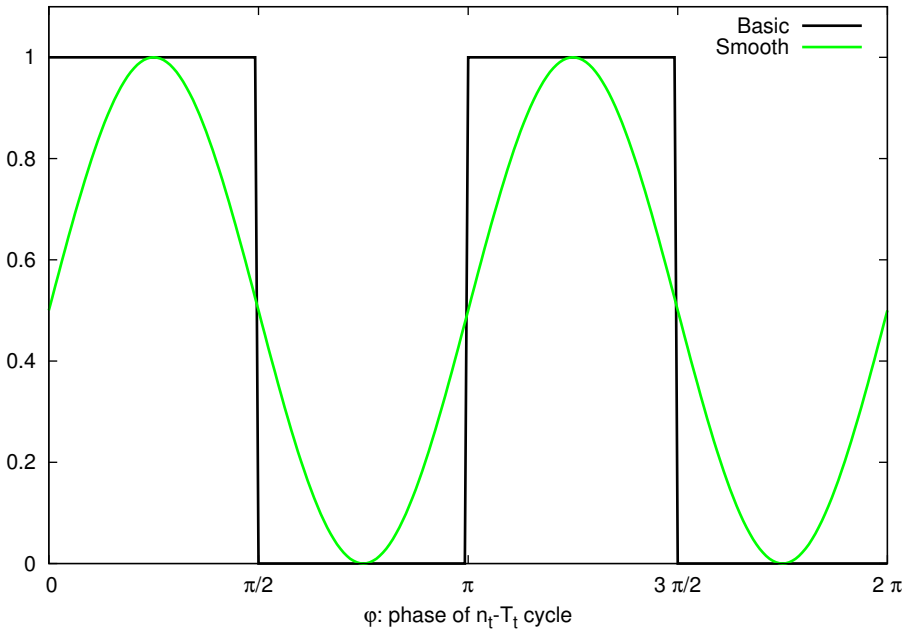

Figure 3.11.: Filter for adaptive relaxation based on the phase of a n_t-T_t cycyle.

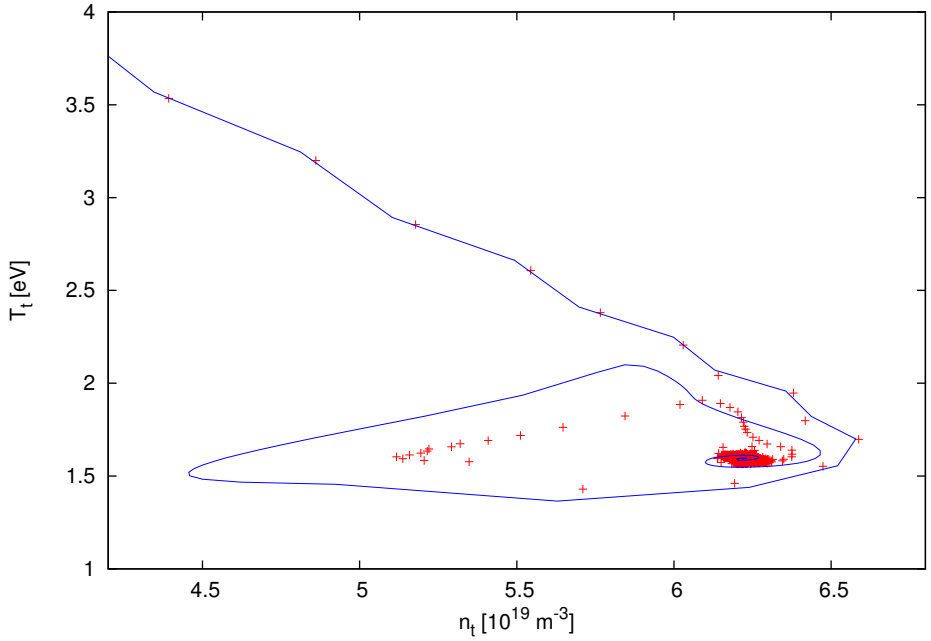

Figure 3.12.: The iterated two-point model in n_t-T_t space when adaptive relaxation based on (3.7) is applied: without noise (blue) and with noise (red).

4. Conclusions

The application of transport solvers for the plasma boundary of magnetic fusion devices has been related to the iterative approximation of a fixed-point of a non-linear map. It has been demonstrated by a simple two-point model that unstable behavior (discrete and continuous oscillations) can occur. Large scale simulations based on more elaborate plasma edge transport models can exhibit similar behavior which must be controlled. An adaptive relaxation scheme has been presented which allows to stabilize the fixed-point iteration. However, implementing an adaptive relaxation scheme into 3D edge plasma simulations leaves plenty of room for optimizations. The present results demonstrate the potential of this method and motivate further benchmarks and advancements.

A. EMC3-EIRENE

Steady state model equations for the plasma edge (n: plasma density, $u_\parallel$: parallel flow velocity, T_e: electron temperature, T_i: ion temperature) as solved by the EMC3-code are:

Particle balance:

$$\nabla \cdot \left[n u_\parallel \mathbf{e}_\parallel - D_\perp \underline{\mathbf{I}}_\perp \cdot \nabla n \right] = S_p \tag{A.1}$$

Momentum balance:

$$\nabla \cdot \mathbf{e}_\parallel \left[m_i n u_\parallel^2 - \eta \, \mathbf{e}_\parallel \cdot \nabla u_\parallel \right] - \nabla \cdot \underline{\mathbf{I}}_\perp \cdot D_\perp \nabla \left(m_i n u_\parallel \right) = -\mathbf{e}_\parallel \cdot \nabla p + S_m \tag{A.2}$$

Electron energy balance:

$$\nabla \cdot \mathbf{e}_\parallel \left[\frac{5}{2} T_e n u_\parallel - \kappa_e \, \mathbf{e}_\parallel \cdot \nabla T_e \right] - \nabla \cdot \underline{\mathbf{I}}_\perp \cdot \left[\chi_e n \nabla T_e + \frac{5}{2} T_e D_\perp \nabla n \right] = -k \left(T_e - T_i \right) + S_{ee} \tag{A.3}$$

Ion energy balance:

$$\nabla \cdot \mathbf{e}_\parallel \left[\frac{5}{2} T_i n u_\parallel - \kappa_i \, \mathbf{e}_\parallel \cdot \nabla T_i \right] - \nabla \cdot \underline{\mathbf{I}}_\perp \cdot \left[\chi_i n \nabla T_i + \frac{5}{2} T_i D_\perp \nabla n \right] = +k \left(T_e - T_i \right) + S_{ei} \tag{A.4}$$

The local direction of the magnetic field is given by the unit vector $\mathbf{e}_\parallel$, which allows to write the cross-field tensor as $\underline{\mathbf{I}}_\perp = \underline{\mathbf{I}} - \mathbf{e}_\parallel \, \mathbf{e}_\parallel$. The static pressure is given by $p = n \left(T_e + T_i \right)$ and $k = \frac{3 m_e}{m_i} \frac{n}{\tau_e}$. Parallel transport coefficients η, κ_e, κ_i are taken from the classical transport theory by Braginskii [3], while anomalous cross-field transport is taken into account by free model parameters $D_\perp$, χ_e, χ_i and fixed viscosity $\eta_\perp = m_i \, n \, D_\perp$. The sources S_p, S_m, S_{ee} and S_{ei} due to interactions with neutral particles are calculated by the kinetic transport code EIRENE.

The model equations for particles, momentum and energy can be related to the generic Fokker-Planck like form

$$\frac{\partial \mathcal{F}}{\partial t} + \nabla \cdot \left[\mathbf{V} \, \mathcal{F} - \mathbf{D} \cdot \nabla \mathcal{F} \right] = S \tag{A.5}$$

where $\mathbf{D} = D_\parallel \, \mathbf{b} \, \mathbf{b} + D_\perp \left(1 - \mathbf{b} \, \mathbf{b} \right)$ is a diffusion tensor. Because of its intrinsic relation to a stochastic process, it is straigthforward to formulate a Monte Carlo method which

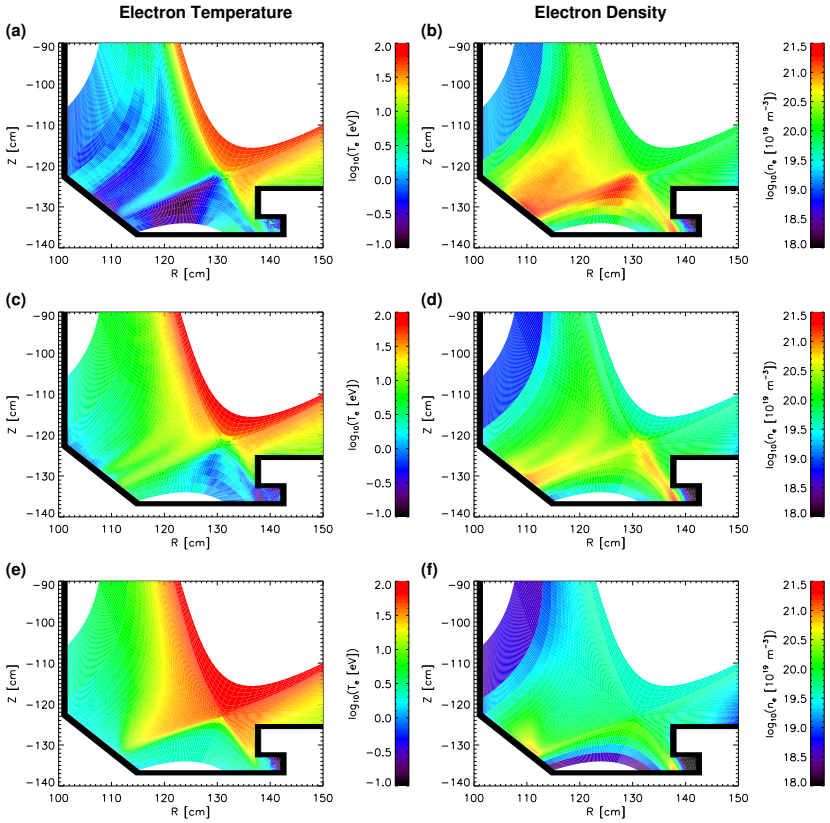

Figure A.1.: Iterated electron temperature and density. Oscillations occur for $\alpha = 0.4$: (a)-(b) intermediate state with low $\overline{T}_{et}$, (c)-(d) intermediate state with high $\overline{T}_{et}$, (e)-(f) converged solution with $\alpha = 0.9$.

solves this type of equation [26]. A magnetic field ($\mathbf{b} = \mathbf{B}/B$) aligned coordinate system is used to separate the fast transport along magnetic field lines from the much slower cross-field transport [27, 16].

Bibliography

[1] Loarte A, *et al.*, 2007 *Nuclear Fusion* **47** S203. doi:10.1088/0029-5515/47/6/S04

[2] Fundamenski W, 2005 *Plasma Phys. Control. Fusion* **47** R163. doi:10.1088/0741-3335/47/11/R01

[3] Braginskii S, 1965 *Review of Plasma Physics* **1** 205

[4] Schneider R, *et al.*, 2006 *Contrib. Plasma Phys.* **46** 1-2 3

[5] Coster D, *et al.*, 2005 *J. Nucl. Mater.* **337-339** 336. doi:10.1016/j.jnucmat.2004.10.013

[6] Kukushkin A, *et al.*, 2003 *Nuclear Fusion* **43** 716. doi:10.1088/0029-5515/43/8/312

[7] Wagner F, *et al.*, 1982 *Phys. Rev. Lett.* **49** 1408. doi:10.1103/PhysRevLett.49.1408

[8] Loarte A, *et al.*, 2003 *Plasma Phys. Control. Fusion* **45** 1549. doi:10.1088/0741-3335/45/9/302

[9] Evans T E, *et al.*, 2004 *Phys. Rev. Lett.* **92** 23 235003. doi:10.1103/PhysRevLett.92.235003

[10] Evans T E, *et al.*, 2006 *Nature Physics* **2** 419. doi:10.1038/nphys312

[11] Liang Y, *et al.*, 2007 *Phys. Rev. Lett.* **98** 265004 1. doi:10.1103/PhysRevLett.98.265004

[12] Suttrop W, *et al.*, 2011 *Phys. Rev. Lett.* **106** 225004. doi:10.1103/PhysRevLett.106.225004

[13] Hawryluk R, *et al.*, 2009 *Nuclear Fusion* **49** 065012. doi:10.1088/0029-5515/49/6/065012

[14] Feng Y, *et al.*, 1999 *Journal of Nuclear Materials* **266-269** 812. doi:10.1016/S0022-3115(98)00844-7

[15] Reiter D, *et al.*, 2005 *Fusion Science and Technology* **47** 2 172

[16] Frerichs H, *et al.*, 2010 *Comp. Phys. Commun.* **181** 61. doi:10.1016/j.cpc.2009.08.016

[17] Frerichs H, *et al.*, 2010 In *37th EPS Conference on Plasma Physics*, P2.127

[18] Frerichs H, *et al.*, 2012 *Phys. Plasmas* **19** 052507. doi:10.1063/1.4714616

[19] Kobayashi M, *et al.*, 2004 *Contrib. Plasma Phys.* **44** 1-3 25. doi:10.1002/ctpp.200410003

[20] Stangeby P, 2000 *The Plasma Boundary of Magnetic Fusion Devices.* Institute of Physics Publishing Bristol and Philadelphia

[21] Kotov V *et al.*, 2009 *Plasma Phys. Control. Fusion* **51** 115002. doi:10.1088/0741-3335/51/11/115002

[22] Frerichs H, *et al.*, 2012 *Nuclear Fusion* **53** 023001. doi:10.1088/0029-5515/52/2/023001

[23] May R M, 1976 *Nature* **261** 459. doi:10.1038/261459a0

[24] ADAS - Atomic Data and Analysis Structure http://www.adas.ac.uk/about.php

[25] Summers H P, *et al.*, 2006 *Plasma Phys. Control. Fusion* **48** 263. doi:10.1088/0741-3335/48/2/007

[26] Feng Y, *et al.*, 2000 In *27th EPS Conference on Contr. Fusion and Plasma Phys.*, volume 24B, pages 1188–1191. Budapest

[27] Feng Y, *et al.*, 2005 *Phys. Plasmas* **12** 052505 1. doi:10.1063/1.1888959

Jül-4368
Dezember 2013
ISSN 0944-2952